Energy & Environmental Science

Microkinetic Model for pH- and Potential-Dependent Oxygen Evolution During Water Splitting on Fe-Doped beta-NiOOH

Journal:	*Energy & Environmental Science*
Manuscript ID	EE-ART-07-2020-002292.R1
Article Type:	Paper
Date Submitted by the Author:	14-Sep-2020
Complete List of Authors:	Govind Rajan, Ananth; Princeton University, Mechanical and Aerospace Engineering Carter, Emily; UCLA, Chemical and Biomolecular Engineering

Microkinetic Model for pH- and Potential-Dependent Oxygen Evolution during Water Splitting on Fe-Doped β-NiOOH

*Ananth Govind Rajan[1,2] and Emily A. Carter[1,3,4]**

[1] Department of Mechanical and Aerospace Engineering, Princeton University, Princeton, New Jersey 08544-5263, United States

[2] Present address: Department of Chemical Engineering, Indian Institute of Science, Bengaluru, Karnataka 560012, India

[3] Department of Chemical and Biomolecular Engineering, University of California, Los Angeles, Los Angeles, California 90095-1592, United States

[4] Office of the Chancellor, Box 951405, University of California, Los Angeles, Los Angeles, California 90095-1405, United States

***Corresponding Author:** Emily A. Carter (E-mail: eac@princeton.edu and eac@ucla.edu)

ABSTRACT

Electrochemical water splitting using excess renewable electricity is a CO_2-free synthesis route for sustainable hydrogen production and a renewable-energy storage strategy. Electrolyte pH and electrode potential are key reactor operating conditions used to tune water-splitting kinetics whose influence remains incompletely understood. Here, we develop a microkinetic model, based on the Marcus theory of electron transfer, to predict the anodic oxygen-evolution-reaction (OER) current density (water-splitting rate) as a function of solution pH and electrode potential. Our model offers startling new insights into OER kinetics on Fe-doped β-nickel oxyhydroxide (β-NiOOH), a promising, inexpensive candidate for electrocatalyzing the OER, under alkaline solution

conditions. Only four fitting parameters with clearly defined physical meaning – reorganization free energies (λ) for H^+- and OH^--based reactions and work terms (w) for transporting H^+/OH^- ions and water from the bulk solution to the electrocatalyst surface – are required to reproduce experimental polarization curves (i.e., current-density vs. potential plots) at multiple alkaline pHs. The inclusion of work terms renders multiple steps rate-determining for the OER. The predicted $\lambda_{H^+} =$ 0.744 eV is much smaller than $\lambda_{OH^-} =$ 2.474 eV, and $w_{ions} =$ 0.607 eV is much larger than $w_{water} =$ 0.065 eV, suggesting that the OER occurs primarily but not exclusively via water oxidation, rather than hydroxide oxidation, even under alkaline conditions. We show unequivocally that hydroxide oxidation also must occur as a minor channel, as accurate reproduction of polarization curves is impossible without it. We conclusively demonstrate the need to use the reversible, rather than the standard, hydrogen electrode as a reference in microkinetic models. Moreover, we deduce that the electrocatalyst surface is positively charged, contrary to inferences made in previous reports. Finally, we predict the following properties for the OER under high overpotential ($\gtrsim$ 0.3 V) conditions on Fe-doped β-NiOOH: a Tafel slope of ~76 mV/decade, an effective charge transfer coefficient of 0.77, and an exchange current density of 3.5 μA/cm^2 rivaling that of RuO_2, one of the best noble-metal-containing water-splitting electrocatalysts. Our work substantially deepens the mechanistic understanding of water-splitting kinetics on inexpensive iron/nickel-oxyhydroxide-based electrocatalysts, which may help optimize operating conditions for their widespread deployment.

BROADER CONTEXT

Thwarting the advances of global warming, caused by continued increases in greenhouse gas emissions, is a major challenge for humankind. Carbon dioxide (CO_2) released during industrial processes is a major contributor to rising temperatures. For example, the conventional production

of hydrogen, an important feedstock used to hydrotreat biomass and petroleum, synthesize ammonia for fertilizer, and produce clean electricity in fuel cells, entails CO_2 release into the atmosphere. Accordingly, developing inexpensive, CO_2-emission-free methods to produce hydrogen at scale, primarily through the electrolysis of water, is of great interest. Despite vigorous research efforts, materials that can efficiently and cost-effectively split water into its constituent elements are hard to come by. Such discovery efforts are further complicated by the lack of understanding as to how important electrolyzer operating conditions, such as electrolyte pH and electrode potential, modulate water splitting. Indeed, an optimal combination of both catalyst material and electrolyzer operating conditions will be required for widespread commercial adoption of water splitting to produce hydrogen. In this work, we directly address the knowledge gap in understanding the effect of electrolyzer operating conditions on water-oxidation kinetics. Water oxidation, i.e., oxygen evolution, is the more difficult half-reaction involved in water splitting. We develop a simple, yet robust framework to quantify how solution pH and electrode potential – two important reactor operating conditions – affect the oxygen evolution reaction (OER), by combining the celebrated Marcus theory of electron transfer with the well-founded transition state theory of reaction kinetics. The resultant model presents remarkable agreement with experimental current-density–electrode-potential–solution pH curves and allows us to reach several counter-intuitive conclusions that overthrow conventional assumptions regarding the mechanism of water electrolysis.

TOC Figure

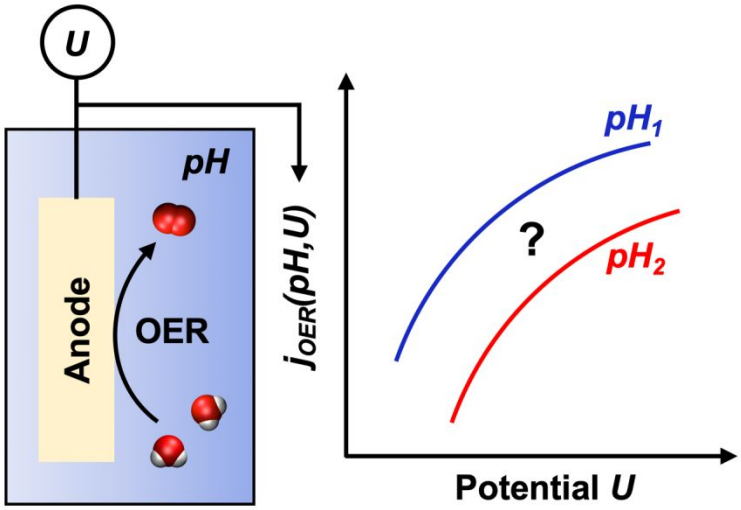

INTRODUCTION

Humankind faces an urgent challenge of thwarting the advances of global warming induced by increased emissions of greenhouse gases, such as carbon dioxide (CO_2). In this regard, water splitting is an important chemical reaction that can enable CO_2-emission-free production of hydrogen gas.[1] Because hydrogen gas can enable clean electricity production via fuel cells and is also a widely used chemical feedstock (e.g., in ammonia/hydrocarbon synthesis and petroleum/biomass hydrotreating), producing it in a carbon-free, on-demand manner is a promising endeavor.[2] Electrochemical water splitting using excess renewable electricity provides a means to produce clean hydrogen and acts as an energy-storage strategy (with the hydrogen produced available as a fuel for future power generation). It involves two half-reactions: the oxygen evolution reaction (OER)[3] and the hydrogen evolution reaction (HER).[4] While alkaline solution conditions favor the OER, acidic solution conditions favor the HER.[5] As a result, some compromise exists between the kinetics of the OER and the HER, because water-splitting reactors must be operated at a constant pH. Moreover, the applied electrode potential significantly affects the hydrogen production rate. Therefore, the system pH and electrode potential are key operating

variables for any water-splitting reactor and understanding how they modulate the electrochemical current density is an important undertaking.[5]

Most quantum-mechanical models of electrocatalytic water splitting focus on reaction thermodynamics, although the use of microkinetic modeling to understand reaction rates has been gaining popularity.[6] The OER is the more difficult half-reaction involved in water splitting due to the involvement of four electron-transfer steps rather than just two in the HER. Thus far, studies have used microkinetic models to understand the potential and pH dependence of the HER.[7–10] However, for the OER, microkinetic models chiefly have examined its potential-dependent kinetics,[7,11–13] with no efforts investigating its pH-dependent kinetics. In one such study directed at the OER, Shinagawa et al. developed microkinetic models for various electrochemical reactions, including the OER, assuming various steps as rate-determining.[7] They were able to predict nonlinear current vs. potential curves with varying Tafel slopes.[7] However, the rate parameters they used were chosen arbitrarily and their plots do not have any numbers on the axes, making their model qualitative in nature, except for the Tafel slopes reported.[7] Xiao et al. developed a microkinetic model for the OER on Fe-doped γ-NiOOH assuming the oxygen-coupling step, a non-electroactive one, as an irreversible process and the sole rate-determining step (RDS).[11] However, microkinetic models ideally should be constructed without assuming any particular step as rate-determining (and the rest at equilibrium) and by considering all the steps in the mechanism as possibly reversible. Further, Xiao et al. did not present polarization curves (i.e., current density vs. potential plots) and only characterized their system using the electrode potential required for an anodic current density of 10 mA/cm^2.[11] In another work, Dickens et al. combined quantum-mechanical density functional theory (DFT) calculations and microkinetic modeling to develop a "kinetic volcano plot" for the OER on various oxide surfaces. The authors thereby demonstrated

the importance of stabilizing the transition state preceding the hydroperoxo intermediate for optimizing OER kinetics.[12] Recently, Mefford et al. combined DFT calculations of Pourbaix (i.e., pH-potential) diagrams and microkinetic modeling to predict the RDS, its rate constant, and its charge transfer coefficient for the OER on $CoO_x(OH)_{2-x}$.[13] However, still no theory exists that describes the pH dependence of OER kinetics.

In contrast to previous theoretical investigations, a number of experimental studies investigated the pH and applied-potential dependence of the OER kinetics on various electrocatalyst surfaces, such as platinum (oxide),[14,15] manganese oxide,[16] cobalt-phosphate,[17] nickel oxide,[18] iridium/cobalt oxide,[19] ruthenium/iridium oxide,[20,21] and iron(Fe)-doped nickel oxyhydroxide (NiOOH).[22–25] In one such study, Louie and Bell collected comprehensive anodic current data on Fe-doped NiOOH, a promising, inexpensive candidate for electrocatalyzing the OER, at various solution pHs between 13.0 and 14.7 and at applied potentials between ~0.4 and 0.7 V vs. the Hg/HgO electrode.[22] These potentials correspond to ~0.498 and 0.798 V vs. the standard hydrogen electrode (SHE). Such extensive current data at varied pHs and potentials allow for complete parametrization of microkinetic models. In this work, we develop a microkinetic model for the OER based on the Marcus and transition state theories of electron transfer and reaction kinetics,[26] respectively, and fit the model using the polarization curves presented in the work of Louie and Bell.[22] The resultant model describes the experimentally observed pH- and potential-dependent OER kinetics well, and provides significant new physical insight into the reaction mechanism operative on the electrocatalyst surface. Specifically, we find that (i) the OER potential-determining step (PDS) derived from thermodynamics need not be the (sole) RDS, (ii) the OER primarily occurs via water rather than hydroxide oxidation even under alkaline solution conditions, (iii) the pH-dependent reversible hydrogen electrode (RHE, *vide infra*), rather than the

SHE, is the appropriate reference electrode to be used in any microkinetic model involving reactions via both H^+ and OH^-, (iv) mixed nickel/iron oxyhydroxide surfaces could be positively charged during the OER, contrary to previous claims in the literature, and (v) the exchange current density of mixed iron/nickel oxyhydroxide rivals that of RuO_2, which is historically one of the best-known water-oxidation electrocatalysts. Further, our microkinetic model for the OER complements previous ones for other electrochemical processes, such as the oxygen reduction reaction (ORR)[27,28] and CO_2 reduction.[29,30]

RESULTS AND DISCUSSION

Basis of the microkinetic model. Our model is based on the Marcus theory of electron transfer.[26,31] According to this theory, the standard Gibbs free energy of activation at applied potential U, $\Delta G^{\ddagger}_{a,fi}(U)$, for a "forward" ($f$) electrochemical process i is related to its standard "Marcus" Gibbs free energy, $\Delta G^{0}_{Marcus,i}(U)$ (Figure 1A):

$$\Delta G^{\ddagger}_{a,fi}(U) = \frac{\lambda_i}{4}\left(1 + \frac{\Delta G^{0}_{Marcus,i}(U)}{\lambda_i}\right)^2 \quad (1)$$

where λ_i is the reorganization free energy, which is the free energy "dissipated when a system that has undergone vertical electron transfer relaxes to the equilibrium state for its new charge distribution."[32] In other words, λ_i is the free energy difference between the reactant and product structural states on the product free energy surface, i.e., after vertical electron transfer occurs (Figure 1A).[26,31]

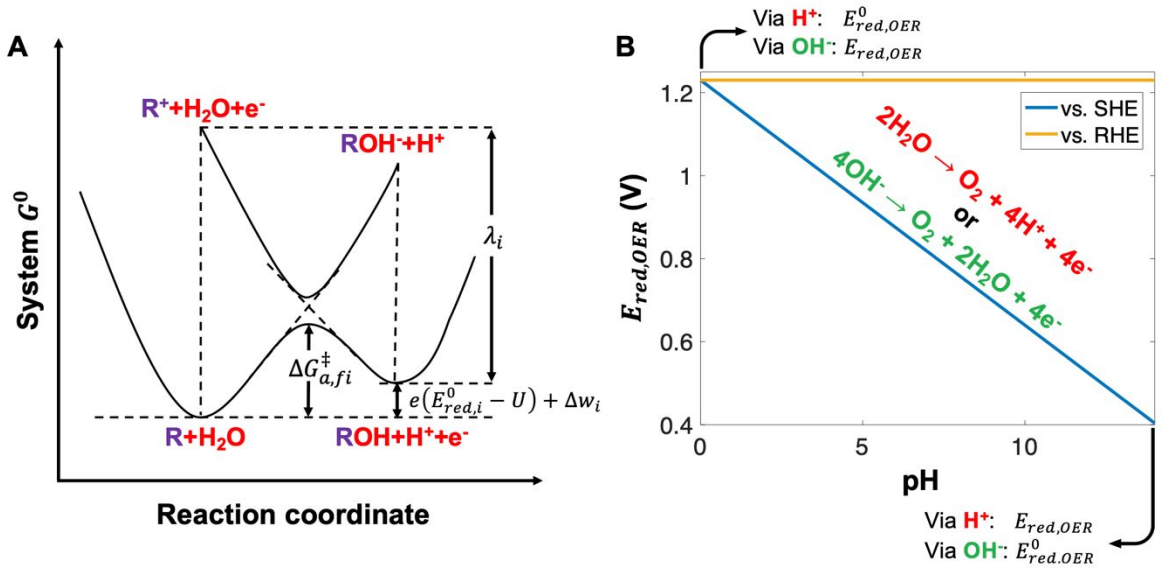

Figure 1. (A) Schematic illustrating the Marcus theory of electrochemical kinetics for the OER at a (photo)anode. For an example oxidation step i, $R + H_2O \rightleftharpoons ROH + H^+ + e^-$, involved in the OER, the reaction coordinate (structure) is shown, with the Gibbs free energy change equal to the standard Gibbs free energy of the reaction, $eE^0_{red,i}$, minus the reduction in the free energy of the electron, eU (where U is the applied potential), plus the *net* (product-reactant) work needed to bring the participating species into the positions required for electron transfer, Δw_i. The standard Gibbs free energy of activation, $\Delta G^{\ddagger}_{a,fi}$, and the reorganization free energy, λ_i, also are indicated. (B) Plot of the OER reduction potential ($E_{red,OER}$) versus the SHE (blue) and RHE (orange) as a function of the pH, indicating that $E_{red,OER}$ does not depend on whether the OER is balanced via H^+ or OH^-. At pH=0, the reaction via H^+ corresponds to standard conditions, i.e., 1 M electrolyte, with an OER reduction potential of 1.23 V (1.23 V) versus the SHE (RHE), while at pH=14, the reaction via OH^- corresponds to standard conditions, with an OER reduction potential of 0.40 V (1.23 V) versus the SHE (RHE).

In Marcus's original formation,[31] $\Delta G^0_{Marcus,i}(U)$ can be related readily to the standard "bulk" Gibbs free energy, $\Delta G^0_{bulk,i}(U)$, as:

$$\Delta G^0_{Marcus,i}(U) = \Delta G^0_{bulk,i}(U) + \Delta w_i \tag{2}$$

where Δw_i denotes the *net* work, $w_p - w_r$, required to bring the products and the reactants from the bulk solution phase to their respective surface states just before electron transfer. We do not include the reactant work term, w_r, as an additive quantity on the right-hand side of Eq. (1), as done originally by Marcus.[31] This is because all kinetic expressions that we formulate (Eq. (8))

involve near-surface concentrations of species and not their bulk concentrations (*vide infra*). If bulk species concentrations were used in the rate expressions, w_r obviously should appear as an additive term in the expression for the standard Gibbs free energy of activation, in addition to the quadratic term, since any work needed to bring the reactants to the surface would increase the free energy of activation. We use standard "bulk" Gibbs free energies for all elementary steps at zero applied potential, $\Delta G^0_{bulk,i}(0)$, calculated using the computational hydrogen electrode (CHE) framework.[33–35] In this framework for *ab initio* thermodynamics, free energies of H_2, O_2, and H_2O are obtained for their standard bulk phases (gas, gas, and liquid, respectively), and that of (H^++e^-) is evaluated as half of that of bulk H_2.[33–35] Although we refer to $\Delta G^0_{bulk,i}(0)$ as the "bulk" free energy, note that one calculates the free energies of adsorbed intermediates on the electrocatalyst *surface* in the CHE framework.

For an elementary oxidation step, the reaction Gibbs free energy decreases with the applied potential, U:

$$\Delta G^0_{Marcus,i}(U) = \Delta G^0_{Marcus,i}(0) - eU \tag{3}$$

where e is the elementary charge on an electron. Furthermore, from the transition state theory of reaction kinetics, the rate constant for an elementary forward reaction i is dependent on temperature as:[26]

$$k_{fi} = \frac{k_B T}{h} \exp\left(-\frac{\Delta G^{\ddagger}_{a,fi}}{k_B T}\right) \tag{4}$$

where k_B denotes the Boltzmann constant, T the system temperature, and h Planck's constant. At room temperature (T=298.15 K), $\frac{k_B T}{h}$ = 6.21 × 10^{12} Hz. Note that we do not use the exact Marcus theory prefactor that depends on the coupling terms between reactants and products (and thereby introduces one or more additional parameters in the model), but instead choose to model the

reaction prefactor using the relatively simpler transition state theory. We fit our model to Louie and Bell's data,[22] collected using a rotating-disk electrode spinning at 2400 rotations per minute (RPM). In that study, the authors showed that the anodic current differs negligibly using a rotation speed of 2000 and 2400 RPM. Therefore, we assume that the electrolyte solution is well-mixed and that there are no transport limitations. Accordingly, the bulk solution concentrations of all molecular/ionic species (i.e., H^+, OH^-, O_2, and H_2O) are equal to their concentrations near the electrode surface. Using Eq. (1) for $\Delta G^{\ddagger}_{a,fi}(U)$ and Eq. (2) for $\Delta G^{0}_{Marcus,i}(U)$ in Eq. (4) for k_{fi}, the rate constant of a forward elementary step i can be written as:

$$k_{fi} = \frac{k_B T}{h} \exp\left(-\frac{\lambda_i}{4 k_B T} \left(1 + \frac{\Delta G^{0}_{bulk,i}(U) + \Delta w_i}{\lambda_i} \right)^2 \right) \tag{5}$$

Previous theoretical work established the importance of modeling the full OER pathway, rather than assuming quasi-equilibrium for the non-rate-determining steps.[36] As a result, we model the complete reaction pathway including backward reactions and assume none of the elementary steps to be in quasi-equilibrium. The OER pathway thermodynamics on Fe-doped β-NiOOH($\bar{1}2\bar{1}1$) elucidated by Martirez and Carter[37] form the basis for our model. Note that Martirez and Carter[37] combined the CHE framework with hybrid DFT calculations using the HSE06 exchange-correlation functional[38] and a system-partitioning scheme[39] to calculate the free energies of the four electron-transfer steps involved in the OER (*vide infra*).

Reduction potential of the OER via OH^-- and H^+-based pathways. The OER can occur via either protons (from water) or via hydroxide ions in solution. The standard reduction potential at room temperature (measured versus the SHE, $E_{SHE} = 0$ V) for the OER balanced using protons (i.e., at pH=0) is 1.23 V, while for the OER balanced using hydroxide ions (i.e., at pH=14), it is 0.40 V. We depict the conversion between the standard reduction potentials of these reactions, through the

free energy for water autoionization, schematically in Figure 2A. What about the reduction potential for the OER at any given pH? Through the Nernst equation, one can show that the reduction potential for the OER is independent of whether the reaction is balanced through H^+ or OH^-; it only depends on pH (see Section S1 of the Electronic Supplementary Information (ESI)). Accordingly, as shown in Figure 1B, a single straight line for both H^+ and OH^- suffices to represent the pH dependence of the OER reduction potential versus the SHE (assuming unit activities for water and oxygen; the conclusion holds for arbitrary water and oxygen activities albeit with a vertically shifted straight-line variation in Figure 1B). Furthermore, the OER reduction potential becomes independent of pH too (constant at 1.23 V, see Figure 1B) if the RHE, $E_{RHE} = -0.059pH$, is used as a reference. In summary, the reduction potential of the OER, E_{OER}, is given as $E_{OER} = (1.23 - 0.059pH)$ V versus the SHE or $E_{OER} = 1.23$ V versus the RHE, irrespective of whether the reactions are balanced using H^+ or OH^-, for unit activities of water and oxygen at room temperature.

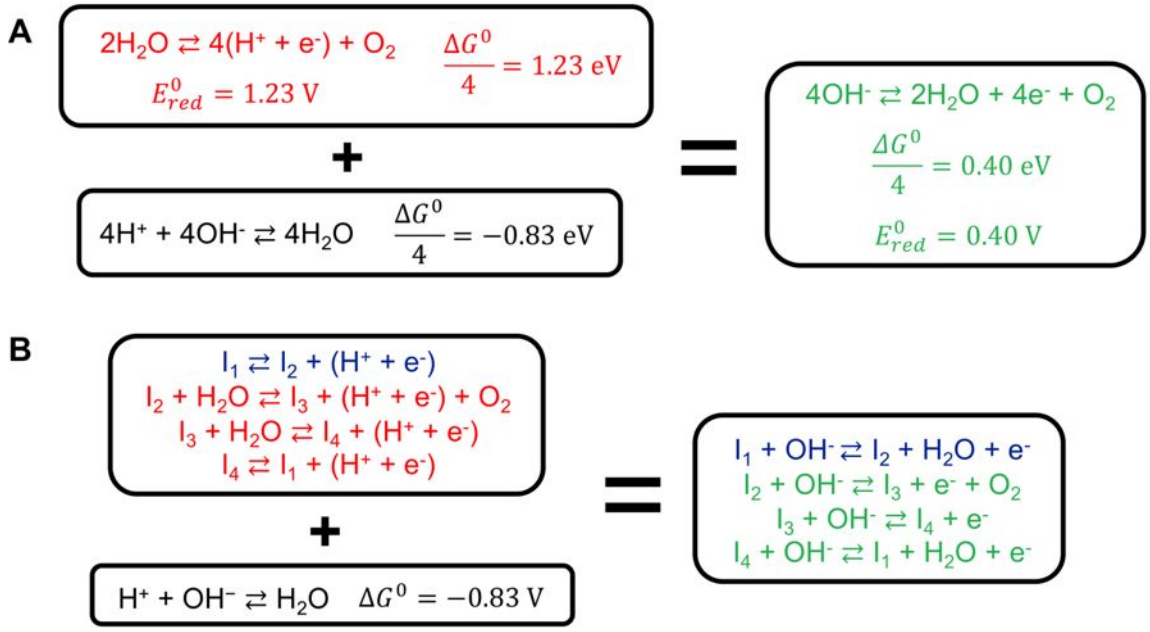

Figure 2. (A) Standard reduction potential of the OER when balanced using H^+ (red), and how it relates to that of the OER balanced using OH^- (green). (B) Conversion of the OER elementary

steps balanced with H^+, adapted from the mechanism proposed by Martirez and Carter,[37] into OER elementary steps balanced with OH^-, by the addition of the reaction corresponding to the inverse auto-ionization of water. The PDSs are shown in blue. Note that I_1 = HO*OH, I_2 = HO*O + $^{\gamma}$OH, I_3 = HO* + $^{\gamma}OH_2$, and I_4 = HO*OH_2, where * represents an adsite (Fe dopant atom on β-NiOOH($\bar{1}2\bar{1}1$)) to which the other species are bonded and $^{\gamma}$ represents a Ni atom in the same layer (an adjacent layer in the [0001] direction) of β-NiOOH.[37]

Training our model using experimental data: Fe-doped β-NiOOH as a case study. Pure and Fe-doped NiOOH are promising electrocatalysts for the OER that are stable under alkaline conditions.[22,40,41] β-NiOOH is a well-characterized phase of NiOOH that has been used successfully in quantum-mechanical modelling of the OER.[42] A number of simulation studies have investigated the thermodynamics of the OER mechanism on various crystallographic facets of pure and Fe-doped β-NiOOH.[37,43–50] The most accurate of such studies[37,49,50] use hybrid DFT,[38] made tractable using a system-partitioning approach,[39] to determine the free energetics of the mechanistic steps comprising the OER. The lowest (and most experimentally consistent, *vide infra*) thermodynamic overpotential predicted for any crystallographic facet of Fe-doped β-NiOOH is 0.14 V, as determined by Martirez and Carter on the Fe-doped ($\bar{1}2\bar{1}1$) facet.[37] Figure 2B explains how the standard free energies for the H^+- and OH^--based elementary steps in the mechanism by Martirez and Carter[37] relate to each other. In this mechanism, all electron-transfer steps are assumed to be proton-coupled electron transfers (PCETs).[51–53] I_1 through I_4 denote adsorbed intermediates, as mentioned in the caption of Figure 2B. Specifically, I_1 is a dihydroxo species (HO*OH), I_2 is a hydroxo-oxo species (HO*O + $^{\gamma}$OH), I_3 is a hydroxo species (HO* + $^{\gamma}OH_2$), and I_4 is a hydroxo-aqua species (HO*OH_2), where * and $^{\gamma}$ denote Fe and Ni atoms in the surface layer.[37] Ni/Fe atoms on the ($\bar{1}2\bar{1}1$) facet are four-fold-lattice-oxygen coordinated, explaining why two adsorbates can adsorb simultaneously at the adsite. Table 1 lists the standard reduction potentials of each elementary step in their mechanism when balanced with H^+ or OH^-, versus the SHE and RHE. Govind Rajan and Carter systematically showed that this mechanism is

the lowest overpotential one on Fe-doped β-NiOOH($\bar{1}2\bar{1}1$) by making use of a newly developed scheme for OER pathway enumeration.[54] The reactions in Table 1 are listed in two forms – without and with a proton-accepting water molecule. We explain the physical significance of these two forms later. For the OER, a number of experimental studies have revealed that a current density of 10 mA/cm^2 requires an applied overpotential, η, of 0.29 V when the electrolyte pH is ~13-14.[22,40,41] However, a single data point for the current density and the applied potential are not sufficient to determine all kinetic model parameters. As a result, we utilize the complete set of polarization curves presented by Louie and Bell[22] at various alkaline pHs to parametrize our model (*vide infra*).

Table 1. Standard "bulk" reduction potentials, $E^0_{bulk,red,i}$, for all of the elementary steps involved in the OER mechanism on Fe-doped β-NiOOH($\bar{1}2\bar{1}1$), adapted from Martirez and Carter.[37] Values are given versus both the SHE and the RHE, with the two sets of values related using Eq. (26). The reactions are listed in two forms – with and without a proton-accepting water molecule.

Label i	Reaction i (without a proton-accepting water molecule)	Reaction i (with a proton-accepting water molecule)	$E^0_{bulk,red,i}$ (V vs. SHE)	$E^0_{bulk,red,i}$ (V vs. RHE)
Reactions through H^+				
1,H^+	$I_1 \rightleftarrows I_2 + (H^+ + e^-)$	$I_1 + H_2O \rightleftarrows I_2 + (H_3O^+ + e^-)$	1.37	1.37
2,H^+	$I_2 + H_2O \rightleftarrows I_3 + (H^+ + e^-) + O_2$	$I_2 + 2H_2O \rightleftarrows I_3 + (H_3O^+ + e^-) + O_2$	1.23	1.23
3,H^+	$I_3 + H_2O \rightleftarrows I_4 + (H^+ + e^-)$	$I_3 + 2H_2O \rightleftarrows I_4 + (H_3O^+ + e^-)$	1.31	1.31
4,H^+	$I_4 \rightleftarrows I_1 + (H^+ + e^-)$	$I_4 + H_2O \rightleftarrows I_1 + (H_3O^+ + e^-)$	1.00	1.00
Reactions through OH^-				
1,OH^-	$I_1 + OH^- \rightleftarrows I_2 + H_2O + e^-$	$I_1 + OH^- \rightleftarrows I_2 + H_2O + e^-$	0.54	1.37
2,OH^-	$I_2 + OH^- \rightleftarrows I_3 + e^- + O_2$	$I_2 + OH^- \rightleftarrows I_3 + e^- + O_2$	0.40	1.23
3,OH^-	$I_3 + OH^- \rightleftarrows I_4 + e^-$	$I_3 + OH^- \rightleftarrows I_4 + e^-$	0.48	1.31
4,OH^-	$I_4 + OH^- \rightleftarrows I_1 + H_2O + e^-$	$I_4 + OH^- \rightleftarrows I_1 + H_2O + e^-$	0.17	1.00

Determining the OER current density using a steady-state reaction-network analysis. The current density can be related to the rates of the elementary steps in the OER mechanism. While writing the rates of the elementary steps, the concentration of the proton-accepting water molecule also needs to be included in the rate expression. As a result, the reactions listed in column 3 of Table 1 are the relevant ones with respect to formulating reaction kinetics. The forward rate

constant for the i^{th} elementary step, k_{fi}, in terms of the forward reaction activation free energy is given using Eq. (4). Furthermore, the forward ($\Delta G^{\ddagger}_{a,fi}$) and backward ($\Delta G^{\ddagger}_{a,bi}$) reaction activation free energies can be related as:

$$\Delta G^{\ddagger}_{a,fi}(U) - \Delta G^{\ddagger}_{a,bi}(U) = \Delta G^{0}_{Marcus,i}(U) = \Delta G^{0}_{bulk,i}(U) + \Delta w_i \tag{6}$$

Therefore, one can readily calculate the backward rate constant for the i^{th} elementary step, k_{bi}, as:

$$k_{bi} = \frac{k_B T}{h} \exp\left(-\frac{\Delta G^{\ddagger}_{a,bi}}{k_B T}\right) \tag{7}$$

The forward rate of any elementary reaction i, r_{fi}, is then given as:

$$r_{fi} = k_{fi} \prod_{l=1}^{n_r} a_{li}^{|\nu_{li}|} \tag{8}$$

where Π denotes a product over all the n_r species participating as reactants in elementary step i, l a reactant in that elementary step, a_{li} the surface activity of the l^{th} reactant (=bulk activity for molecular/ionic species, due to the assumption of no transport limitations), and ν_{li} the signed stoichiometric coefficient of the l^{th} reactant (negative for reactants). The backward rate of any elementary reaction i can be written similarly.

The activity of water (a_{H_2O}) is given by its mole fraction in solution; that of O_2 (a_{O_2}) by its aqueous concentration normalized by its standard concentration (i.e., at 1 bar pressure); that of H^+ (or H_3O^+; $a_{H^+} = a_{H_3O^+}$) by the ratio of its molar concentration to the standard molar concentration (1 M); that of OH^- (a_{OH^-}) by the ratio of its molar concentration to the standard molar concentration (1 M); and that of each surface species I_l (a_{I_l}) by its surface fraction θ_l, defined as the ratio of its active surface concentration to its standard surface concentration:

$$a_{H_2O} = \frac{C^0_{H_2O}}{C^0_{H_2O} + a_{H^+} + a_{OH^-} + C_{O_2(aq)}} \quad (9)$$

$$a_{O_2} = \frac{C_{O_2(aq)}}{C^0_{O_2}} \quad (10)$$

$$a_{H^+} = a_{H_3O^+} = \frac{10^{-pH}\ \mathrm{M}}{1\ \mathrm{M}} \quad (11)$$

$$a_{OH^-} = \frac{K_W a_{H_2O}}{a_{H^+}} \quad (12)$$

$$a_{I_l} = \theta_l = \frac{C_{I_l}}{C_{sites}} \quad (13)$$

where $C^0_{H_2O}$ (=55.34 M) is the molarity of pure water at room temperature, $C_{O_2(aq)}$ is the saturation concentration of dissolved O_2 in water (calculated to be 2.69×10^{-4} M, using a room temperature solubility,[55] S_{O_2}, of 1.28×10^{-3} M/atm O_2 and a partial pressure in air, $p_{O_2,air}$, of 0.21 atm), $C^0_{O_2}$ is the standard concentration of O_2 gas at room temperature (calculated to be 4.03×10^{-2} M using the ideal gas law: $C^0_{O_2} = \frac{p^0}{RT}$, with R being the universal gas constant and p^0 = 1 bar), K_W is the equilibrium constant for the auto-ionization of water (=1.01×10^{-14} at room temperature[56]), C_{I_l} is the surface concentration of the l^{th} surface species, and C_{sites} denotes the total number of active sites (Fe ions) on the Fe-doped β-NiOOH surface (*vide infra*). Note that equations (9) and (12) need to be solved self-consistently to get the values of a_{H_2O} and a_{OH^-}. Further, in Eq. (13), C_{sites} appears in the denominator because in the CHE calculations of Martirez and Carter,[37] the standard

state of each surface species involved the sole Fe active site in the simulation supercell having that species adsorbed on it, implying that C_{sites} adsorbates would exist per unit area in the standard state. Although we have used here the solubility of O_2 in pure water, one could consider its solubility in an appropriate concentration of KOH in the microkinetic model. However, in Section S2 of the ESI, we show that the medium in which O_2 is assumed to be dissolved does not affect the OER current density significantly under the conditions we have considered. Moreover, there is a distinct advantage of using the O_2 solubility in pure water as we have done to parametrize the microkinetic model. Namely, the data in the literature for O_2 solubility in aqueous KOH solutions[57] are only available for three temperatures – 0 °C, 25 °C, and 60 °C – implying that any predictions of the OER current density would be restricted to these temperatures if the model is not based on O_2 solubility in pure water.

Based on the reaction network presented in column 3 of Table 1, we can formulate the temporal rate of change of the intermediate concentrations using ordinary differential equations as follows:

$$\frac{d\theta_1}{dt} = \left(-k_{f1,H^+}\theta_1 a_{H_2O} + k_{b1,H^+}\theta_2 a_{H^+}\right) + \left(k_{f4,H^+}\theta_4 a_{H_2O} - k_{b4,H^+}\theta_1 a_{H^+}\right) + \left(-k_{f1,OH^-}\theta_1 a_{OH^-} + k_{b1,OH^-}\theta_2 a_{H_2O}\right) + \left(k_{f4,OH^-}\theta_4 a_{OH^-} - k_{b4,OH^-}\theta_1 a_{H_2O}\right) \quad (14)$$

$$\frac{d\theta_2}{dt} = \left(-k_{f2,H^+}\theta_2 a_{H_2O}^2 + k_{b2,H^+}\theta_3 a_{H^+} a_{O_2}\right) + \left(k_{f1,H^+}\theta_1 a_{H_2O} - k_{b1,H^+}\theta_2 a_{H^+}\right) + \left(-k_{f2,OH^-}\theta_2 a_{OH^-} + k_{b2,OH^-}\theta_3 a_{O_2}\right) + \left(k_{f1,OH^-}\theta_1 a_{OH^-} - k_{b1,OH^-}\theta_2 a_{H_2O}\right) \quad (15)$$

$$\frac{d\theta_3}{dt} = \left(-k_{f3,H^+}\theta_3 a_{H_2O}^2 + k_{b3,H^+}\theta_4 a_{H^+}\right) + \left(k_{f2,H^+}\theta_2 a_{H_2O}^2 - k_{b2,H^+}\theta_3 a_{H^+} a_{O_2}\right) + \left(-k_{f3,OH^-}\theta_3 a_{OH^-} + k_{b3,OH^-}\theta_4\right) + \left(k_{f2,OH^-}\theta_2 a_{OH^-} - k_{b2,OH^-}\theta_3 a_{O_2}\right) \quad (16)$$

$$\frac{d\theta_4}{dt} = \left(-k_{f4,H^+}\theta_4 a_{H_2O} + k_{b4,H^+}\theta_1 a_{H^+}\right) + \left(k_{f3,H^+}\theta_3 a_{H_2O}^2 - k_{b3,H^+}\theta_4 a_{H^+}\right) + \left(-k_{f4,OH^-}\theta_4 a_{OH^-} + k_{b4,OH^-}\theta_1 a_{H_2O}\right) + \left(k_{f3,OH^-}\theta_3 a_{OH^-} - k_{b3,OH^-}\theta_4\right) \quad (17)$$

In each of these equations, the first two parenthetical terms on the right-hand side correspond to reactions through H^+ and the next two parenthetical terms correspond to reactions through OH^-. Positive and negative signs denote production and consumption of surface intermediates, respectively. The subscript for each reaction corresponds to the labels listed in Table 1. At steady state, temporal derivatives of all adsorbed intermediate concentrations will be zero, i.e., $\frac{d\theta_l}{dt} = 0$. The resultant set of linear equations can be solved simply by matrix inversion. To do that, we include a site balance equation instead of the fourth steady-state (dependent) eq. (17):

$$\sum_{l=1}^{4} \theta_l = 1 \quad (18)$$

Upon solving for θ_1 through θ_4, the OER current density, j_{OER}, can be obtained as:

$$j_{OER} = \sum_{i=1}^{4} \left(\left(r_{fi,H^+} - r_{bi,H^+}\right) + \left(r_{fi,OH^-} - r_{bi,OH^-}\right)\right) e C_{sites} \quad (19)$$

Calculating the active site density on Fe-doped β-NiOOH. As an important parameter in our model, the active site density, C_{sites}, must be specified *a priori*. Martirez and Carter found that the most-active facet of Fe-doped β-NiOOH is the $(\bar{1}2\bar{1}1)$ facet, because it demonstrates a very low

thermodynamic OER overpotential of only 0.14 V.[37] So far, only this theoretical value offers a consistent lower bound for the measured overpotential of ~0.29 V at a current density of 10 mA/cm^2 and a pH of ~14.[22,40,41] Out of 1 m^2 of β-NiOOH, only $\left(\begin{matrix}\text{area}\\ \text{fraction}\end{matrix}\right)_{(\bar{1}2\bar{1}1)}$ m^2, i.e., 0.015 m^2 is occupied by the $(\bar{1}2\bar{1}1)$ facet as determined by the Wulff construction method.[58] From the crystal structure of the $(\bar{1}2\bar{1}1)$ facet, each nickel atom occupies 24.4 Å^2 of space on average (including the empty space around it).[58] Therefore, in 1 m^2 of β-NiOOH (i.e., 0.015 m^2 of the $(\bar{1}2\bar{1}1)$ facet), 6.14×10^{16} Ni atoms will exist. In Louie and Bell's dataset used in this work, Fe dopes 37% of the surface Ni atoms, implying 2.27×10^{16} Fe atoms exist in 1 m^2 of area. This thus corresponds to an active site density, C_{sites}, of 2.27×10^{12} cm^{-2}.

Determining and rationalizing Marcus theory parameters for the OER on Fe-doped β-NiOOH. We carried out a least-squares fitting of the anodic current density to obtain the Marcus theory parameters – reorganization free energies and *net* work terms (for more details, see the Methods section). The parameters are grouped together based on physical justification presented in Figure 3; overall, our model involves four fitting parameters (*vide infra* for justification regarding why four parameters are sufficient). We assume that two separate reorganization free energies (Figure 1A) for reactions via H^+ and OH^- (Figure 3A), i.e., λ_{H^+} and λ_{OH^-}, respectively, are sufficient to describe all the elementary steps involved (*vide infra* for fit quality based on this assumption). To illustrate the physical meaning of λ_{H^+} and λ_{OH^-}, we consider an example elementary step R + $H_2O \rightarrow$ ROH + H^+ + e^- (equivalently, R + OH^- $\rightarrow$ ROH + e^-) where R represents the electrocatalyst. For these reactions, λ_{OH^-} is the free energy difference between R^++OH^-+e^- and ROH+e^- and λ_{H^+} is the analogous quantity between R^++H_2O+e^- and ROH+H^++e^-. The notation R^++OH^-+e^- (R^++H_2O+e^-) denotes that an electron has been lost by the electrocatalyst R to form R^+, but the

structure has not yet relaxed to form the final state, i.e., ROH+e^- (ROH+H^++e^-). Such an electron transfer is a "vertical" electron transfer on the free energy diagram (Figure 1A) and obeys the Franck-Condon principle.[59]

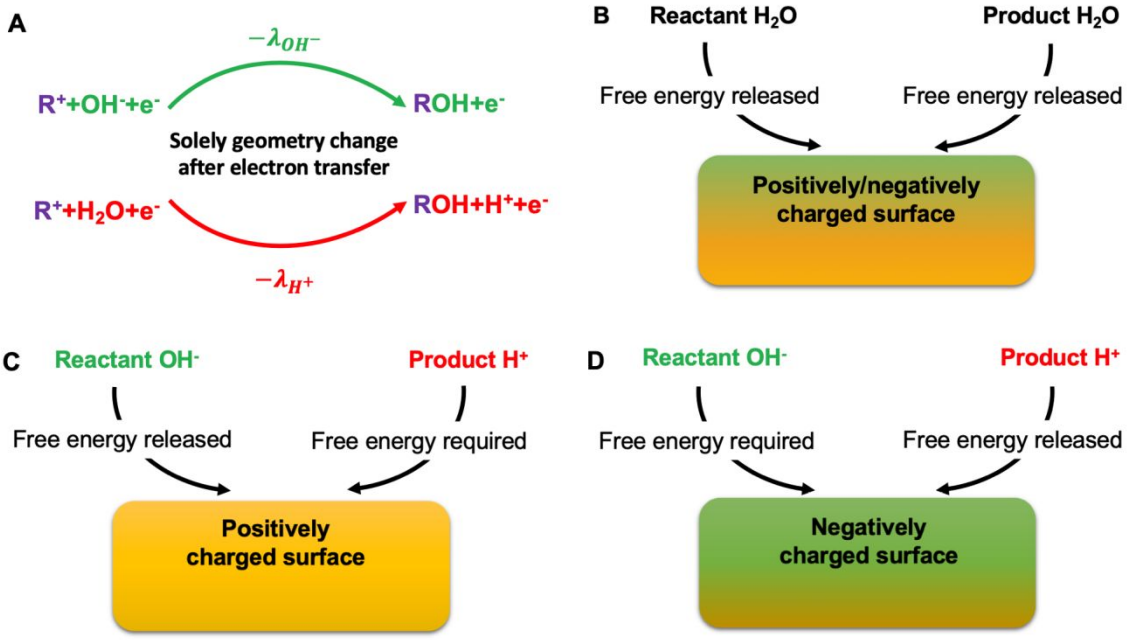

Figure 3. Physical justification for the parameters used in our Marcus-theory-based microkinetic model. (A) The reorganization free energy (λ) is the free energy change between the reactant and the product structural state on the product free energy surface. For the OH^--based pathway (green), the relevant species would be R^++OH^-+e^- and ROH+e^- and for the H^+-based pathway (red), they would be R^++H_2O+e^- and ROH+H^++e^-. In (B)-(D), the incoming arrows indicate that the transport of both reactants and products *towards* the surface is used to define the work done. (B) Irrespective of the charge on the surface, a water molecule (a dipole) is attracted to it, causing the *net* (product minus reactant) work to be equal in magnitude, but opposite in sign, when water is involved as a product or as a reactant (by releasing energy during adsorption in both cases); see text for more detail. (C) A positively charged electrocatalyst surface would attract OH^-, a reactant, and repel H^+, a product. Thereby the *net* work done to bring both the products and reactants to the surface (indicated by the incoming arrows) would roughly be the same for OH^- and H^+; see text for more detail. (D) Similar justifications hold for a negatively charged electrocatalyst surface that would repel OH^-, a reactant, and attract H^+, a product.

Furthermore, we use two separate work terms for water (w_{water}) and ions (w_{ions}), because different amounts of work would be involved in transporting water and H^+/OH^- ions to the electrocatalyst surface. Work terms are required for both reactants and products because the CHE model calculates thermodynamics using bulk free energies, rather than adsorbed-state free energies (*vide*

supra). Furthermore, because the *net* work term ($w_p - w_r$) appears in the Marcus free energy, both reactant and product work terms are defined with respect to transport *from the bulk to the surface*, even though in reality any products will move from the surface to the bulk after the reaction. (If ($-w_p - w_r$) appeared in the Marcus free energy, product work terms would be defined with respect to transport from the surface to the bulk.) Note that we did not include the water molecules involved as proton acceptors (i.e., precursors to H_3O^+) while writing the *net* work terms (product work minus reactant work), as these water molecules are not "consumed" or "produced" during the process. Indeed, the product protons can simply diffuse away from the surface by the Grotthuss (proton-hopping) mechanism,[60] with the adsorbed water molecules staying in place. As a result, the reactions listed in column 2 of Table 1 are used for determining work terms. As shown in Figure 3B, irrespective of whether the electrocatalyst surface is positively/negatively charged, work $-w_{water}$ ($w_{water} > 0$) would be required to move a *reactant* H_2O (a dipole) towards the charged surface (reactions 2,H^+ and 3,H^+). The *net* work in this case for moving water molecules would be $0 - (-w_{water}) = w_{water}$. The product work term is zero in the preceding equation because water is not involved as a product in reactions 2,H^+ and 3,H^+ (see column 2 in Table 1). For moving a *product* H_2O towards the charged surface (reactions 1,OH^- and 4,OH^-), the *net* work would be $-w_{water} - 0 = -w_{water}$. The reactant work term is zero in the preceding equation because water is not involved as a reactant in reactions 1,OH^- and 4,OH^-. Moreover, for reactions 1,H^+; 4,H^+; 2,OH^-; and 3,OH^- in Table 1, no water molecules are involved as reactant/product (except for a proton-accepting one), and thus the *net* work term related to water adsorption is zero.

Next, we consider the work terms involved in transporting ions to the electrocatalyst surface. For this, we examine two separate cases based on whether the surface is assumed to be positively or negatively charged. If the surface were positively charged (Figure 3C), OH^- would

be attracted towards the surface (work expended = $-w_{ions}$; $w_{ions} > 0$) and H^+ would be repelled by it (work expended = w_{ions}). Accordingly, transporting OH^-, a reactant ($0 - (-w_{ions}) = w_{ions}$) and transporting H^+, a product ($w_{ions} - 0 = w_{ions}$) would both result in a positive *net* work term. In the preceding equations, the product and reactant work terms respectively are zero because OH^- and H^+ are not involved as products and reactants, respectively, in any reaction. Similarly, if the surface were negatively charged (Figure 3D), both transporting OH^-, a reactant ($0 - w_{ions} = -w_{ions}$) and transporting H^+, a product ($-w_{ions} - 0 = -w_{ions}$) would result in a negative *net* work term. Note that w_{ions} is assumed to be positive in sign in the above discussion.

As a result, work terms for ions are independent of whether the reactions are balanced using H^+ or OH^-, because irrespective of the charge on the electrocatalyst surface, bringing closer or taking away an OH^- (a reactant) or H^+ (a product), respectively, would entail similar free energy changes, whose magnitude we assume to be w_{ions}. Based on the above discussion, the *net* work term associated with any elementary step i can be written as:

$$\Delta w_i = w_{ions} - \nu_{water,i} w_{water} \quad (20)$$

where $\nu_{water,i}$ represents the signed stoichiometric coefficient of water in reaction i while not including a proton-accepting water (column 2 in Tables 1 and 2). For example, $\nu_{water} = 1$ for reactions involving water as a product (1,OH^- and 4,OH^-), and $\nu_{water} = -1$ for reactions involving water as a reactant (2,H^+ and 3,H^+). Because ions are involved in each of the reactions, w_{ions} is included without any multiplying term in the expression for Δw_i. The work terms for water and ions in each reaction, based on Eq. (20), are summarized in Table 2. The sign of w_{ions} depends on the sign of the charge on the electrode (*vide supra*). $\Delta G^0_{Marcus,i}(0)$ values listed in Table 2 are

calculated via Eq. (2) using the corresponding $\Delta G^0_{bulk,i}(0)$ value from the CHE model[37] and the *net* work term from Eq. (20). Note that w_{ions} = 0.607 eV and w_{water} = 0.065 eV, *vide infra*. As an example, for reaction 2,H^+ in Table 2, $\Delta w_{2,H^+} = w_{ions} + w_{water}$ = 0.672 eV, such that $\Delta G^0_{Marcus,2,H^+}(0) = \Delta G^0_{bulk,2,H^+}(0) + \Delta w_{2,H^+}$ = 1.902 eV.

Table 2. Standard "bulk" and "Marcus" reaction Gibbs free energies (i.e., without and with *net* work terms included), $\Delta G^0_{bulk,i}(0)$ (adapted from ref. 37) and $\Delta G^0_{Marcus,i}(0)$, respectively, at zero applied potential, for all the elementary steps involved in the OER mechanism on Fe-doped β-NiOOH($\bar{1}2\bar{1}1$). The work terms for water and ions are indicated for each reaction.

Label *i*	Reaction *i* (without a proton-accepting water molecule)	Ion work term	Water work term	$\Delta G^0_{bulk,i}(0)$ (eV)	$\Delta G^0_{Marcus,i}(0)$ (eV)
1,H^+	$I_1 \rightleftarrows I_2 + (H^+ + e^-)$	w_{ions}	0	1.37	1.98
2,H^+	$I_2 + H_2O \rightleftarrows I_3 + (H^+ + e^-) + O_2$		w_{water}	1.23	1.90
3,H^+	$I_3 + H_2O \rightleftarrows I_4 + (H^+ + e^-)$		w_{water}	1.31	1.98
4,H^+	$I_4 \rightleftarrows I_1 + (H^+ + e^-)$		0	1.00	1.61
1,OH^-	$I_1 + OH^- \rightleftarrows I_2 + H_2O + e^-$		$-w_{water}$	0.54	1.08
2,OH^-	$I_2 + OH^- \rightleftarrows I_3 + e^- + O_2$		0	0.40	1.01
3,OH^-	$I_3 + OH^- \rightleftarrows I_4 + e^-$		0	0.48	1.09
4,OH^-	$I_4 + OH^- \rightleftarrows I_1 + H_2O + e^-$		$-w_{water}$	0.17	0.71

Based on the groupings of the parameters described above, we carried out least-squares fitting of the net anodic current density obtained from Eq. (19) to the current-density–electrode-potential–pH data from Louie and Bell[22] (see Methods section and Figure 4). To evaluate Eq. (19), various inputs are required – forward rate constants from Eq. (5), backward rate constants from Eq. (7), forward/backward reaction rates from Eq. (8), activities of the molecular/ionic/adsorbed species from Eqs. (9) through (13), steady-state adsorbate coverages from Eqs. (14) through (18) by setting temporal concentration derivatives to zero, and *net* work terms for each reaction listed in Table 1 using Eq. (20). In terms of the physical parameters entering these equations, the temperature is set to 298.15 K, $\Delta G^0_{bulk,i}(0)$ is adapted from quantum-mechanical calculations presented by Martirez and Carter[37] (see Table 2), and C_{sites} is set to the value determined above.

We use the appropriate pH and electrode potential corresponding to each data point from Louie and Bell (Figure 4).[22] Note that the reorganization free energies for H^+/OH^--based reactions (λ_{H^+} and λ_{OH^-}) and the work terms for water and ion transport (w_{water} and w_{ions}) constitute the four fitting parameters in our model. We used the RHE as the reference electrode in our microkinetic model, with the applied potentials, U, and the standard reaction potentials, $E^0_{bulk,red,i}$, referenced using active and standard pHs, respectively (see Eqs. (25) and (26)). In Section S3 of the ESI, we explain why using the RHE as a reference electrode is essential for any microkinetic model involving reactions via both H^+ and OH^-. Therein, we also offer proof that using the SHE as a reference electrode leads to a poorer fit of the microkinetic model to experimental data and leads to unphysical model parameter values.

Following the fitting procedure (see Methods section), we obtained a low root-mean-square deviation (RMSD, see Eq. (24)) of 0.26, between the model-predicted and experimental[22] anodic current densities. The measured and fitted polarization curves are shown in Figure 4, indicating good agreement between experimental data[22] and the proposed model involving only four fitting parameters, for all pH values, except pH=13.3. We note that if the experimental pH corresponding to those data points was 13.4 or 13.5 instead of 13.3, the fit would be much better, leading to a much-lower RMSD of 0.201 or 0.195, respectively (see Section S4 in the ESI). As a result, the less favorable agreement between the predicted and measured OER current densities for pH=13.3 could be attributed to a small error of ~0.1-0.2 in the measured pH. It seems that the model not only matches experimental data satisfactorily, it also allows us to uncover systematic errors in the measurements used to parameterize it! Further, the predicted polarization curves are consistent with the understanding that the OER is more favorable at higher pH, because the current density increases with pH for a fixed applied potential (vs. the Hg/HgO electrode or the SHE). The

best-fit parameters along with their 90% confidence intervals are given in Table 3. The low values of the confidence intervals indicate that the obtained parameter values are reliable. The quality of the fit is also indicated by our calculated overpotential of ~0.28 V for a current density of 10 mA/cm^2 at pH=14 being very close to the measured value of ~0.29 V for the same current density in various studies.[22,40,41] Recall that the standard OER reduction potential at pH=14 is 0.40 V versus the SHE (U_{SHE}), such that it is 0.302 V versus the Hg/HgO electrode ($U_{Hg/HgO}$), because $U_{SHE} = U_{Hg/HgO} + 0.098$. Accordingly, one can verify that at a potential of (0.302 V + 0.28 V) = 0.582 V and pH=14, the current density is ~10 mA/cm^2 in Figure 4.

To check the robustness of our model and the assumed grouping of parameters, we carried out the fitting process with different numbers of model parameters than considered here. We present three more cases in Section S5 in the ESI, corresponding to the use of five, ten, and eleven fitting parameters. Therein, we show that consideration of an increased number of parameters does not improve the fit RMSD significantly; rather it makes confidence intervals very wide, leads to unphysical parameter values in some instances, and does not alter the *qualitative* conclusion that $\lambda_{H^+} < \lambda_{OH^-}$.

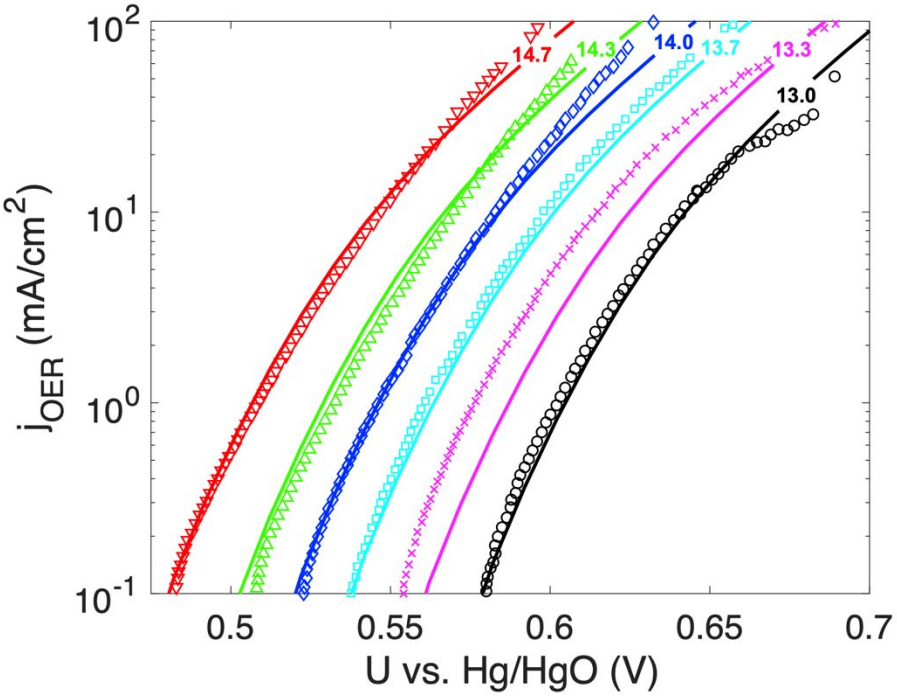

Figure 4. Comparison of the model fit (solid lines) and the experimentally measured polarization curves (symbols) for the OER on Fe-doped NiOOH at various alkaline pH values ranging from 13.0 to 14.7 (color code: black – 13.0, magenta – 13.3, cyan – 13.7, blue – 14.0, green – 14.3, red – 14.7). Experimental data is shown using various symbols (13.0 – circles, 13.3 – crosses, 13.7 – squares, 14.0 – diamonds, 14.3 – upward triangles, and 14.7 – downward triangles) and is adapted from the study by Louie and Bell.[22]

Table 3. Marcus theory parameters and their 90% confidence intervals for the OER on Fe-doped β-NiOOH($\bar{1}2\bar{1}1$) determined by fitting to experimental data.

Parameter	Value (eV)
w_{ions}	0.607 ± 0.054
w_{water}	0.065 ± 0.017
λ_{H^+}	0.744 ± 0.219
λ_{OH^-}	2.474 ± 0.174

One can rationalize physically why $w_{ions} > w_{water}$ because the absolute values of the work involved would be larger when transporting ions (charged entities), rather than water molecules (uncharged dipolar entities), to the electrocatalyst surface. The positive value obtained for w_{water} indicates that the assumed signs for the work terms for water as a reactant/product are correct. Further, the positive value obtained for w_{ions} indicates that the electrocatalyst surface is positively

charged during the OER (Figure 3C). We offer reasons as to why this may be true, even at alkaline pH, wherein one might expect OH^- to adsorb onto the electrocatalyst surface, thereby imparting it negative charge. First, a positive potential is applied to the anode during the operation of an electrolytic cell, so that the anode could be positively charged throughout. Second, a number of holes will be present in the anode at steady-state (especially so in a semiconductor like NiOOH) to combine with electrons being released by the oxidant, imparting, as a result, positive charge to the anode. However, a number of studies involving surface-enhanced Raman spectroscopy (SERS) have postulated a negative charge on NiOOH during the OER.[23,61,62] These studies offered the following three *plausible* reasons for a negatively charged surface: (i) a strong pH dependence of the OER on the material, (ii) the pH of zero charge being around 12.0 for NiOOH, such that the surface would have a negative charge above the pH of zero charge, and (iii) the electrocatalyst likely undergoing simultaneous OH^- adsorption, deprotonation, and electron loss to form an OOH^- group during the OER cycle.

Instead, our model shows that the surface need not be negatively charged to be consistent with the experimentally observed pH dependence of the OER kinetics. Secondly, at a pH above the point of zero charge, the surface could still be positively charged due to the application of a positive potential to the anode. Finally, deprotonation and OH^- adsorption might not occur concomitantly as redox reactions typically either involve H^+ or OH^-, but not both. As a result, one of two scenarios could occur: $*OH \rightarrow *O + (H^+ + e^-)$ followed by $*O + H_2O \rightarrow *OOH + (H^+ + e^-)$ or $*OH + OH^- \rightarrow *O + H_2O + e^-$ followed by $*O + OH^- \rightarrow *OOH + e^-$, both leading to a neutral O group, rather than OOH^- on the electrocatalyst surface despite deprotonation. Any of the two scenarios leading to a negatively charged hydroperoxo group – $*OH + OH^- \rightarrow *OOH^- + (H^+ + e^-)$ or $*O + OH^- \rightarrow *OOH^-$ – would be unlikely because the former possibility involves a proton

(hydroxide ion) escaping from (incorporating into) a negatively charged surface and the latter one is a non-electroactive step leading to a negatively charged group that would be unstable under the oxidizing conditions of the OER.

We also attempted to understand the variation of the OER current density with applied potential and solution pH under acidic/neutral/mildly alkaline conditions. To this end, we plotted OER polarization curves for pHs 0, 2, 4, 6, 7, 8, 10, and 12, as shown in Section S6 of the ESI. We find that at lower pH, a higher applied potential is required to obtain positive OER current densities, as compared to a higher pH. This is because H^+ is a product in each reaction of the OER and a high H^+ concentration (low pH) leads to an increased reverse reaction rate. At higher applied potentials, this effect is counteracted by the reduced thermodynamic free energies for oxidation reactions, due to the lowered free energy of an electron on the electrode surface. Although these results are interesting, NiOOH is not particularly stable under low pH conditions due to acid-induced dissolution,[63] indicating that one should be cautious while interpreting the predicted OER current densities for pH $\leq$ 7. Indeed, with respect to OER (photo)electrocatalysts, only noble-metal-containing ones, such as RuO_2 and IrO_2, are stable in acidic media.[5,64]

Understanding the steady-state surface coverage of Fe-doped β-NiOOH during the OER. Figure 5 depicts the fractional occupation of the Fe-doped $(\bar{1}2\bar{1}1)$ surface by the four different intermediates (I_1 through I_4) in our considered mechanism at steady state. We see that the concentrations of the four intermediates show different behavior with increasing applied potential. While I_1 first increases and then decreases in surface coverage with increasing applied potential (versus the Hg/HgO electrode) in the studied range, I_3 first decreases and then increases in surface coverage with increasing applied potential. On the other hand, I_2 displays monotonically increasing coverage with increasing applied potential. Further, the coverage of I_2 is much lower than that of

I_1 and I_3. Finally, I_4 always occupies a negligible fraction of the active sites, which is even lower than the surface coverage of I_2.

We can explain these *qualitatively* different behaviors based on the net rates of each of the four elementary steps. While the first step is in principle the PDS from a CHE viewpoint (by having the highest $\Delta G^0_{bulk,i}(0)$ in Table 2), upon including *net* work terms, both the first and third steps effectively become RDSs (having the highest $\Delta G^0_{Marcus,i}(0)$ values in Table 2). Further, the rate of the second step will be higher than the rates of the first and the third steps due to a lower value of $\Delta G^0_{Marcus,i}(0)$. Finally, the fourth step will be quickest, due to having the lowest value of $\Delta G^0_{Marcus,i}(0)$ among the four steps. Using the above facts, we offer a physical reason for why the orders of magnitude, O, of the surface fractions are in the order: $O(\theta_1) \approx O(\theta_3) > O(\theta_2) > O(\theta_4)$. The coverages of I_1 and I_3 are the largest among the four surface species because the steps producing them (4 and 2, respectively) are faster compared to the steps consuming them (1 and 3, respectively). Because the second step which consumes I_2 is faster than the first step which produces it, the surface coverage of I_2 is comparatively lower ($O(10^{-2})$). In fact, the fourth step which consumes I_4 is much faster compared to the third step which produces it, such that the surface coverage of I_4 ($O(10^{-4})$) the lowest among all surface species.

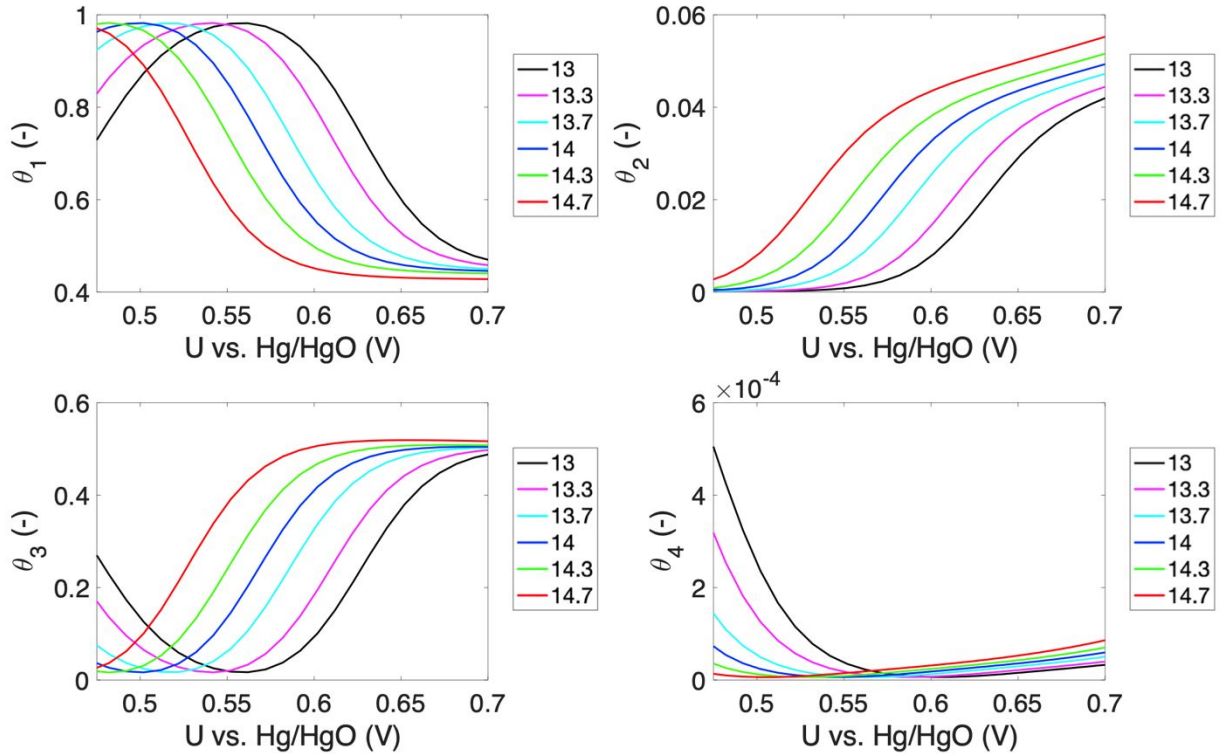

Figure 5. Steady-state fractional occupation of the Fe-doped $(\bar{1}2\bar{1}1)$ surface of β-NiOOH by the four different intermediates in our considered mechanism at various applied potential and pH values. pH increases from right to left, such that the rightmost (black) curve represents pH=13.0 and the leftmost (red) curve represents pH=14.7.

Next, we discuss the distinct shapes of the θ_l vs U curves for the four surface species. This discussion is based on the principle that the rate of a given reaction depends not only on its rate constant, but also on the concentrations of the participating species. We split our discussion into two parts: (i) for the lower three pHs considered (i.e., 13.0, 13.3, and 13.7) and (ii) for the three higher pHs considered (i.e., 14.0, 14.3, and 14.7), since qualitatively different trends are observed for the θ_l vs U curves for these two cases (Figure 5).

In the former case (i), at low applied potentials, only the fourth step would have an appreciable rate (because of its lowest $\Delta G^0_{Marcus,i}(0)$). As a result, I_1 will build up more as the applied potential increases, leading to an increase in θ_1. Simultaneously, I_4 will get consumed more, leading to a decrease in θ_4. Further, the I_4 getting converted to I_1 would have to be

replenished by more of it being produced from I_3. Accordingly, θ_3 decreases with applied potential. Conversely, the increased buildup of I_1 would lead to a larger production of I_2, causing θ_2 to increase with applied potential. However, at higher applied potentials, the second step (which has the next lowest $\Delta G^0_{Marcus,i}(0)$ and produces I_3) also will start to occur at an appreciable rate, leading to an increase in θ_3 as the applied potential increases and explaining the minima in the θ_3 vs. U curves. Concomitantly, I_2 being depleted to produce I_3 would slow down the former's rate of increase with increasing applied potential (observed as a change in slope of the θ_2 vs. U curve). Moreover, I_2 will have to be replenished by increasing consumption of I_1, leading to a reduction in θ_1 with potential and explaining the maxima in the θ_1 vs. U curves. As the applied potential further increases, the first and the third step will also start having considerable rates, leading to further depletion of I_1 and a saturation of I_3, and the concomitant buildup of I_2 to its maximum concentration on the surface.

In the latter case (ii), since the increased pH will accelerate the rates of all steps, there is no "first phase" where only the fourth/second steps have an appreciable rate. Accordingly, there is no prominent maxima (minima) in the θ_1 (θ_3/θ_4) curves and the discussion presented in the previous paragraph for large potentials is applicable. Finally, we rationalize why coverage curves for higher solution pH are shifted to the left, notwithstanding the change in shape of the θ_l vs. U curves with pH as discussed above. Because of the use of the Hg/HgO electrode as a reference, a given potential with respect to the RHE (a pH-independent scale) would correspond to a lower potential with respect to the Hg/HgO electrode at higher pH (*vide infra*, Eq. (25)).

Relative rates of H^+- and OH^--mediated OER on Fe-doped β-NiOOH. To quantify the fraction of the total OER current density (j_{OER}) that is attributable to protons versus hydroxide ions in

solution, we calculated the respective current densities, j_{OER,H^+} and j_{OER,OH^-} for the same operating conditions as in Figure 4 using the following equations:

$$j_{OER,H^+} = \sum_{i=1}^{4} (r_{fi,H^+} - r_{bi,H^+}) e C_{sites} \quad (21)$$

$$j_{OER,OH^-} = \sum_{i=1}^{4} (r_{fi,OH^-} - r_{bi,OH^-}) e C_{sites} \quad (22)$$

Using Eqs. (21) and (22), Figure 6 plots j_{OER,H^+} and j_{OER,OH^-} as a function of the applied potential (vs. the Hg/HgO electrode) at various alkaline solution pHs. From Figure 6, we observe that $j_{OER,H^+} \gg j_{OER,OH^-}$ at most of the applied potential and pH combinations considered in this work, indicating that the OER occurs primarily via protons on Fe-doped β-NiOOH even under alkaline solution conditions – a very counter-intuitive observation. This finding is rationalized by the much smaller reorganization free energy for reactions to occur via H^+ (λ_{H^+}) than for them to occur via OH^- (λ_{OH^-}); see Table 3. To check the robustness of our conclusion, we also carried out fits of the microkinetic model to experimental data with the H^+- or OH^--based elementary steps excluded from the reaction network (see Section S7 of the ESI). We found that the fit is very poor when the OER is assumed to occur solely via OH^-. The fit is marginally better when the OER is assumed to occur solely via H^+. The best fit demonstrating nonlinear polarization curves, however, occurs only when reactions involving both H^+ and OH^- are considered, as discussed above, with $\lambda_{H^+} < \lambda_{OH^-}$, thereby indicating a subtle combination of the kinetics of both sets of reactions to yield the observed polarization curves.

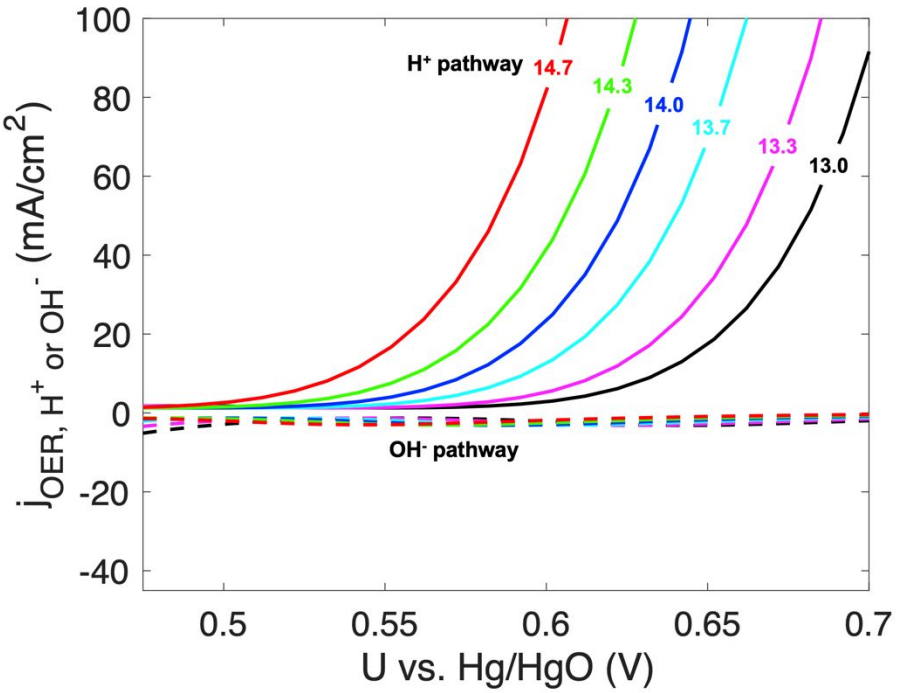

Figure 6. OER current densities attributed to H^+ (solid lines) and OH^- (dashed lines) pathways at various applied potential and pH values. The rightmost (black) curve represents pH=13.0 and the leftmost (red) curve represents pH=14.7.

Tafel analysis for the OER on Fe-doped β-NiOOH. We also calculated several metrics relevant to characterizing OER kinetics on Fe-doped β-NiOOH. We found mean Tafel slopes (over the six alkaline pH values considered in this study) of:

- 26.2 mV/decade to increase the current density ten-fold from 0.1 mA/cm^2,
- 37.9 mV/decade to increase it ten-fold from 1 mA/cm^2,
- 61.6 mV/decade to increase it ten-fold from 10 mA/cm^2, and finally,
- 78.0 mV/decade to increase it ten-fold from 100 mA/cm^2.

These values are derived from the data in Figure 4 (although current densities beyond 100 mA/cm^2 are not shown there) and are consistent with the general understanding that Tafel slopes increase with increasing current density. Although we can define the Tafel slope at low overpotentials (and current densities), it only makes physical sense at high applied overpotentials. This is because the

Tafel equation (Eq. (23)) assumes the backward reaction rate to be negligible compared to the forward reaction rate and the current density to be determined solely by the RDS. Both of these assumptions are only valid at high applied overpotentials. (Note that the Tafel equation assumes that there are no mass-transfer limitations in solution, an assumption that is implicit in our model.) At high current densities, we can express the overpotential through the Tafel equation as:

$$\eta = \frac{2.303 k_B T}{\alpha e} \log_{10}\left(\frac{j}{j_0}\right) \quad (23)$$

where $2.303 = \ln 10$, α denotes the charge transfer coefficient, e the elementary charge, and j_0 the "exchange" current density, which is the extrapolated current density at zero applied overpotential. To determine the charge transfer coefficient and the exchange current density, we plot the applied overpotential versus $\log_{10}$(OER current density) for all the pH values considered in this study in Figure 7, and focus on the region of high overpotential, in which this plot is linear.

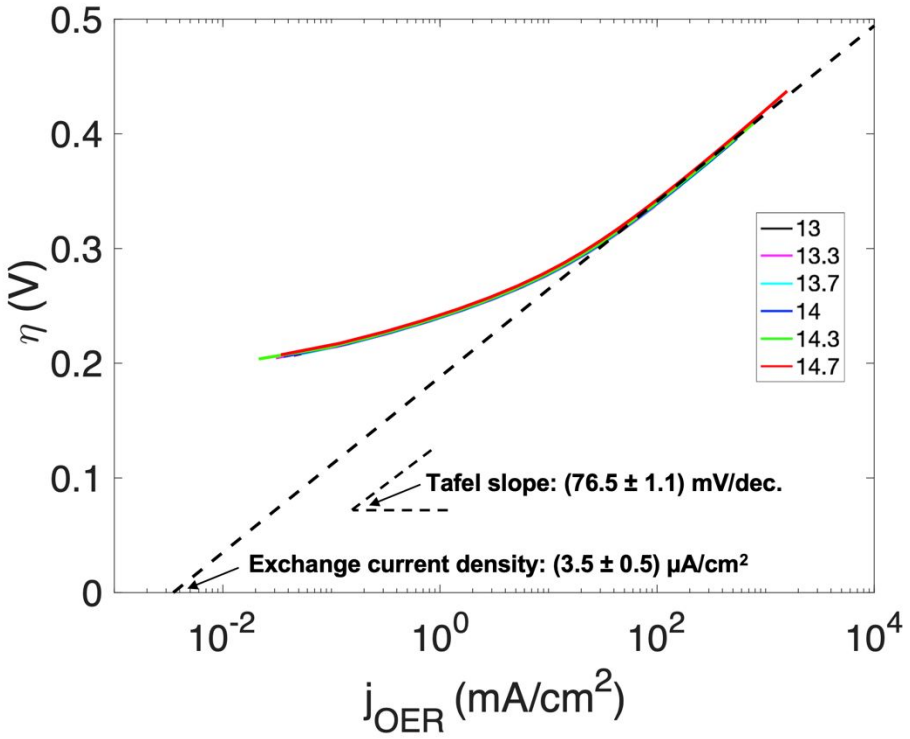

Figure 7. Tafel analysis for Fe-doped β-NiOOH using the microkinetic model presented in this work. The applied overpotential is plotted vs. the OER current density for various solution pHs. Subsequently, the high overpotential region data is fit to a linear equation (dashed black line) to obtain the Tafel slope and the exchange current density. The error range for the Tafel slope is a 90% confidence interval.

From the linear region of this plot ($j > 30$ mA/cm^2), we determine through a least-squares fit (R^2=0.996), the charge transfer coefficient α to be 0.77 ± 0.01 (from the Tafel slope of (76.5 ± 1.1) mV/decade) and the exchange current density j_0 to be around (3.5 ± 0.5) μA/cm^2 (from the horizontal intercept). Details on how the errors in α and j_0 were estimated are provided in Section S8 of the ESI. Our estimate for the exchange current density of Fe-doped β-NiOOH lies in the range of that quantity for one of the best known OER electrocatalysts, RuO_2 (~1 to 10 μA/cm^2).[1] The higher the exchange current density is for a material and process, the more facile the electrochemical process is, when catalyzed by that material. Accordingly, our model and the ensuing Tafel analysis are consistent with the general consensus that Fe-doped β-NiOOH is a particularly promising OER electrocatalyst.

CONCLUSIONS

In this work, by combining the Marcus theory of electron transfer and the transition state theory of reaction kinetics, we developed a microkinetic model to describe the pH and electric-potential dependence of the OER. Our model involves four fitting parameters that have clearly defined physical meaning and provides good agreement with experimental polarization curves at various alkaline pHs. The four parameters are the reorganization free energies for reactions through H^+ and OH^- and the work terms for transporting ions and water to the electrocatalyst surface. We provided reliable estimates and confidence intervals for these parameters, and rationalized the mathematical signs of these parameters. Furthermore, we showed that the RHE, rather than the SHE, is the appropriate reference electrode to be used in microkinetic models that include reactions

mediated by both H^+ and OH^-. Moreover, contrary to interpretations of previous experimental work, our model implies that Fe-doped β-NiOOH is positively charged under the conditions of the OER. Additionally, we showed, consistent with experimental data, that the OER is favored more as pH increases due to concentration-dependent rate effects (when using pH-independent reference electrodes, e.g., the Hg/HgO electrode and SHE). Surprisingly, we found that the OER occurs primarily via water oxidation, rather than hydroxide oxidation, even under alkaline pHs. Nevertheless, we showed that both sets of reactions – water and hydroxide oxidation – are essential to reproduce the nonlinear OER polarization curves seen experimentally, indicating a subtle interplay between the two sets of reactions. Finally, we also determined several experimentally relevant metrics for the OER on Fe-doped β-NiOOH, such as the Tafel slope, the charge transfer coefficient, and the exchange current density. We showed that the exchange current density for the OER on mixed Ni/Fe oxyhydroxide rivals that of RuO_2, one of the best-known water-oxidation electrocatalysts. While we use Marcus theory to estimate activation free energies from reaction free energies, future work could consider determining activation free energies in a fully *ab initio* manner. Our work advances the understanding of how pH and electrode potential can be tuned to achieve the desired OER current density on Fe-doped β-NiOOH in particular and water-splitting (photo)anodes in general. Accordingly, we hope that both theorists and experimentalists use our framework to better link reactor operating conditions and water-splitting kinetics with the goal of enabling controlled water splitting in a commercial setting.

METHODS

We carried out least-squares fitting to determine the model parameters in MATLAB R2017a using the `lsqnonlin` function, with the maximum numbers of objective function evaluations and iterations set to 10,000 and 2,000, respectively. The upper and lower bounds for the reorganization

free energies were set to 3 eV and 0 eV, respectively, and for the *net* work terms to 2 eV and -2 eV, respectively, because the latter parameters can be negative. We determined the 90% confidence intervals on the parameters using the `nlparci` function available in MATLAB R2017a and the system Jacobian returned by the `lsqnonlin` function. We defined the objective function, S, as the sum-of-squares of the relative error between the measured and predicted values as:

$$S = \sum_{m=1}^{N_d} \left(\frac{j_{expt} - j_{pred}}{j_{expt}} \right)^2 \quad (24)$$

where m denotes an experimental observation, N_d the total number of data points, j_{expt} the measured current density at a given value of the solution pH and applied potential U, and j_{pred} the predicted current density at the same value of the solution pH and applied potential. The experimental data in Figure S11(b) of the Supporting Information provided by Louie and Bell[22] was digitized using the WebPlotDigitizer tool,[65] resulting in a total of 408 data points. During the fitting process, the applied potentials were referenced to the RHE. Because the applied potentials reported by Louie and Bell were referenced to the Hg/HgO electrode ($U^{expt}_{Hg/HgO}$), they were referenced to the RHE (U^{expt}_{RHE}) using the experimental pH as follows:

$$U^{expt}_{RHE} = U^{expt}_{Hg/HgO} + 0.098 + 0.059pH \quad (25)$$

The standard reaction potentials were also referenced to the RHE (see Table 1 above and Section S3 of the ESI), but using the standard pH^0, as follows:

$$E^0_{bulk,red,i,RHE} = E^0_{bulk,red,i,SHE} + 0.059pH^0 \quad (26)$$

where $pH^0 = 0$ for reactions through H^+ and $pH^0 = 14$ for reactions through OH^-. Accordingly, as shown in Table 1, all four elementary steps have the same respective $E^0_{bulk,red,i,RHE}$, whether written via H^+ or OH^-.

ELECTRONIC SUPPLEMENTARY INFORMATION

(S1) Equivalence of the OER reduction potentials for H^+- and OH^--based pathways; (S2) why we use the solubility of oxygen in pure water, rather than in aqueous KOH, in our model; (S3) why we use the RHE as the reference electrode in the proposed microkinetic model; (S4) a plausible explanation for why the predicted and measured polarization curves do not agree as well for pH=13.3; (S5) why the proposed microkinetic model has four fitting parameters; (S6) using the microkinetic model to inform OER kinetics under acidic/neutral/mildly alkaline solution conditions; (S7) whether we can conclusively say that the reorganization free energy is lower for reactions involving H^+ than for reactions involving OH^-; and (S8) error determination for the charge transfer coefficient and exchange current density obtained from the Tafel analysis.

CONFLICTS OF INTEREST

There are no conflicts of interest to declare.

ACKNOWLEDGEMENTS

We thank Dr. Sai Gautam Gopalakrishnan and Dr. John Mark P. Martirez for useful discussions on the Butler-Volmer theory of electrode kinetics/economics of water splitting and the Marcus theory of electron transfer, respectively. Additionally, we thank Ms. Samantha Luu for proofreading a detailed outline of this manuscript. E. A. C. acknowledges financial support from the Air Force Office of Scientific Research under AFOSR Award No. FA9550-14-1-0254.

REFERENCES

(1) Walter, M. G.; Warren, E. L.; McKone, J. R.; Boettcher, S. W.; Mi, Q.; Santori, E. A.; Lewis, N. S. Solar Water Splitting Cells. *Chem. Rev.* **2010**, *110*, 6446–6473.

(2) Brown, D. US and World Hydrogen Production — 2014. *CryoGas International* **2016**.
(3) Suen, N.-T.; Hung, S.-F.; Quan, Q.; Zhang, N.; Xu, Y.-J.; Chen, H. M. Electrocatalysis for the Oxygen Evolution Reaction: Recent Development and Future Perspectives. *Chem. Soc. Rev.* **2017**, *46*, 337–365.
(4) Zeng, M.; Li, Y. Recent Advances in Heterogeneous Electrocatalysts for the Hydrogen Evolution Reaction. *J. Mater. Chem. A* **2015**, *3*, 14942–14962.
(5) Govind Rajan, A.; Martirez, J. M. P.; Carter, E. A. Why Do We Use the Materials and Operating Conditions We Use for Heterogeneous (Photo)Electrochemical Water Splitting? *ACS Catal.* In Press, DOI: 10.1021/acscatal.0c01862.
(6) Marshall, A. T. Using Microkinetic Models to Understand Electrocatalytic Reactions. *Curr. Opin. Electrochem.* **2018**, *7*, 75–80.
(7) Shinagawa, T.; Garcia-Esparza, A. T.; Takanabe, K. Insight on Tafel Slopes from a Microkinetic Analysis of Aqueous Electrocatalysis for Energy Conversion. *Sci. Rep.* **2015**, *5*, 13801.
(8) Haghighat, S.; Dawlaty, J. M. pH Dependence of the Electron-Transfer Coefficient: Comparing a Model to Experiment for Hydrogen Evolution Reaction. *J. Phys. Chem. C* **2016**, *120*, 28489–28496.
(9) Rebollar, L.; Intikhab, S.; Snyder, J. D.; Tang, M. H. Determining the Viability of Hydroxide-Mediated Bifunctional HER/HOR Mechanisms through Single-Crystal Voltammetry and Microkinetic Modeling. *J. Electrochem. Soc.* **2018**, *165*, J3209–J3221.
(10) Lamoureux, P. S.; Singh, A. R.; Chan, K. pH Effects on Hydrogen Evolution and Oxidation over Pt(111): Insights from First-Principles. *ACS Catal.* **2019**, *9*, 6194–6201.
(11) Xiao, H.; Shin, H.; Goddard, W. A. Synergy between Fe and Ni in the Optimal Performance of (Ni,Fe)OOH Catalysts for the Oxygen Evolution Reaction. *Proc. Natl. Acad. Sci.* **2018**, *115*, 5872–5877.
(12) Dickens, C. F.; Kirk, C.; Nørskov, J. K. Insights into the Electrochemical Oxygen Evolution Reaction with Ab Initio Calculations and Microkinetic Modeling: Beyond the Limiting Potential Volcano. *J. Phys. Chem. C* **2019**, *123*, 18960–18977.
(13) Mefford, J. T.; Zhao, Z.; Bajdich, M.; Chueh, W. C. Interpreting Tafel Behavior of Consecutive Electrochemical Reactions through Combined Thermodynamic and Steady State Microkinetic Approaches. *Energy Environ. Sci.* **2020**, *13*, 622–634.
(14) Birss, V. I. Oxygen Evolution at Platinum Electrodes in Alkaline Solutions: II. Mechanism of the Reaction. *J. Electrochem. Soc.* **1986**, *133*, 1621.
(15) Birss, V. I.; Damjanovic, A. Oxygen Evolution at Platinum Electrodes in Alkaline Solutions I. Dependence on Solution pH and Oxide Film Thickness. *J. Electrochem. Soc.* **1987**, *134*, 113–117.
(16) Mohammad, A. M.; Awad, M. I.; El-Deab, M. S.; Okajima, T.; Ohsaka, T. Electrocatalysis by Nanoparticles: Optimization of the Loading Level and Operating pH for the Oxygen Evolution at Crystallographically Oriented Manganese Oxide Nanorods Modified Electrodes. *Electrochim. Acta* **2008**, *53*, 4351–4358.
(17) Surendranath, Y.; Kanan, M. W.; Nocera, D. G. Mechanistic Studies of the Oxygen Evolution Reaction by a Cobalt-Phosphate Catalyst at Neutral pH. *J. Am. Chem. Soc.* **2010**, *132*, 16501–16509.
(18) Sadiek, I. M.; Mohammad, A. M.; El-Shakre, M. E.; El-Deab, M. S. Electrocatalytic Activity of Nickel Oxide Nanoparticles-Modified Electrodes: Optimization of the Loading Level and Operating pH towards the Oxygen Evolution Reaction. *Int. J. Hydrogen Energy*

2012, *37*, 68–77.
(19) Minguzzi, A.; Fan, F.-R. F.; Vertova, A.; Rondinini, S.; Bard, A. J. Dynamic Potential–pH Diagrams Application to Electrocatalysts for Water Oxidation. *Chem. Sci.* **2012**, *3*, 217–229.
(20) Giordano, L.; Han, B.; Risch, M.; Hong, W. T.; Rao, R. R.; Stoerzinger, K. A.; Shao-Horn, Y. pH Dependence of OER Activity of Oxides: Current and Future Perspectives. *Catal. Today* **2016**, *262*, 2–10.
(21) Stoerzinger, K. A.; Rao, R. R.; Wang, X. R.; Hong, W. T.; Rouleau, C. M.; Shao-Horn, Y. The Role of Ru Redox in pH-Dependent Oxygen Evolution on Rutile Ruthenium Dioxide Surfaces. *Chem* **2017**, *2*, 668–675.
(22) Louie, M. W.; Bell, A. T. An Investigation of Thin-Film Ni–Fe Oxide Catalysts for the Electrochemical Evolution of Oxygen. *J. Am. Chem. Soc.* **2013**, *135*, 12329–12337.
(23) Diaz-Morales, O.; Ferrus-Suspedra, D.; Koper, M. T. M. The Importance of Nickel Oxyhydroxide Deprotonation on Its Activity towards Electrochemical Water Oxidation. *Chem. Sci.* **2016**, *7*, 2639–2645.
(24) Görlin, M.; Gliech, M.; de Araújo, J. F.; Dresp, S.; Bergmann, A.; Strasser, P. Dynamical Changes of a Ni-Fe Oxide Water Splitting Catalyst Investigated at Different pH. *Catal. Today* **2016**, *262*, 65–73.
(25) Görlin, M.; Ferreira de Araújo, J.; Schmies, H.; Bernsmeier, D.; Dresp, S.; Gliech, M.; Jusys, Z.; Chernev, P.; Kraehnert, R.; Dau, H.; *et al.* Tracking Catalyst Redox States and Reaction Dynamics in Ni–Fe Oxyhydroxide Oxygen Evolution Reaction Electrocatalysts: The Role of Catalyst Support and Electrolyte pH. *J. Am. Chem. Soc.* **2017**, *139*, 2070–2082.
(26) Bard, A. J.; Faulkner, L. R. *Electrochemical Methods: Fundamentals and Applications*; Wiley, 2000.
(27) Holewinski, A.; Linic, S. Elementary Mechanisms in Electrocatalysis: Revisiting the ORR Tafel Slope. *J. Electrochem. Soc.* **2012**, *159*, H864–H870.
(28) Fantauzzi, D.; Zhu, T.; Mueller, J. E.; Filot, I. A. W.; Hensen, E. J. M.; Jacob, T. Microkinetic Modeling of the Oxygen Reduction Reaction at the Pt(111)/Gas Interface. *Catal. Letters* **2015**, *145*, 451–457.
(29) Chen, L. D.; Urushihara, M.; Chan, K.; Nørskov, J. K. Electric Field Effects in Electrochemical CO_2 Reduction. *ACS Catal.* **2016**, *6*, 7133–7139.
(30) Singh, M. R.; Goodpaster, J. D.; Weber, A. Z.; Head-Gordon, M.; Bell, A. T. Mechanistic Insights into Electrochemical Reduction of CO_2 over Ag Using Density Functional Theory and Transport Models. *Proc. Natl. Acad. Sci. U. S. A.* **2017**, *114*, E8812–E8821.
(31) Marcus, R. A. On the Theory of Electron-Transfer Reactions. VI. Unified Treatment for Homogeneous and Electrode Reactions. *J. Chem. Phys.* **1965**, *43*, 679–701.
(32) Reorganization Energy in Electron Transfer. In *IUPAC Compendium of Chemical Terminology, 2nd ed. (the "Gold Book")*; McNaught, A. D.; Wilkinson, A., Eds.; Blackwell Scientific Publications: Oxford, 1997.
(33) Nørskov, J. K.; Rossmeisl, J.; Logadottir, A.; Lindqvist, L.; Kitchin, J. R.; Bligaard, T.; Jónsson, H. Origin of the Overpotential for Oxygen Reduction at a Fuel-Cell Cathode. *J. Phys. Chem. B* **2004**, *108*, 17886–17892.
(34) Rossmeisl, J.; Logadottir, A.; Nørskov, J. K. Electrolysis of Water on (Oxidized) Metal Surfaces. *Chem. Phys.* **2005**, *319*, 178–184.
(35) Rossmeisl, J.; Qu, Z.-W.; Zhu, H.; Kroes, G.-J.; Nørskov, J. K. Electrolysis of Water on

Oxide Surfaces. *J. Electroanal. Chem.* **2007**, *607*, 83–89.
(36) Marshall, A. T.; Vaisson-Béthune, L. Avoid the Quasi-Equilibrium Assumption When Evaluating the Electrocatalytic Oxygen Evolution Reaction Mechanism by Tafel Slope Analysis. *Electrochem. commun.* **2015**, *61*, 23–26.
(37) Martirez, J. M. P.; Carter, E. A. Unraveling Oxygen Evolution on Iron-Doped β-Nickel Oxyhydroxide: The Key Role of Highly Active Molecular-like Sites. *J. Am. Chem. Soc.* **2019**, *141*, 693–705.
(38) Krukau, A. V.; Vydrov, O. A.; Izmaylov, A. F.; Scuseria, G. E. Influence of the Exchange Screening Parameter on the Performance of Screened Hybrid Functionals. *J. Chem. Phys.* **2006**, *125*, 224106.
(39) Chung, L. W.; Sameera, W. M. C.; Ramozzi, R.; Page, A. J.; Hatanaka, M.; Petrova, G. P.; Harris, T. V.; Li, X.; Ke, Z.; Liu, F.; *et al.* The ONIOM Method and Its Applications. *Chem. Rev.* **2015**, *115*, 5678–5796.
(40) Klaus, S.; Cai, Y.; Louie, M. W.; Trotochaud, L.; Bell, A. T. Effects of Fe Electrolyte Impurities on $Ni(OH)_2$/NiOOH Structure and Oxygen Evolution Activity. *J. Phys. Chem. C* **2015**, *119*, 7243–7254.
(41) Friebel, D.; Louie, M. W.; Bajdich, M.; Sanwald, K. E.; Cai, Y.; Wise, A. M.; Cheng, M.-J.; Sokaras, D.; Weng, T.-C.; Alonso-Mori, R.; *et al.* Identification of Highly Active Fe Sites in (Ni,Fe)OOH for Electrocatalytic Water Splitting. *J. Am. Chem. Soc.* **2015**, *137*, 1305–1313.
(42) Tkalych, A. J.; Yu, K.; Carter, E. A. Structural and Electronic Features of β-$Ni(OH)_2$ and β-NiOOH from First Principles. *J. Phys. Chem. C* **2015**, *119*, 24315–24322.
(43) Li, Y.-F.; Selloni, A. Mechanism and Activity of Water Oxidation on Selected Surfaces of Pure and Fe-Doped NiO_X. *ACS Catal.* **2014**, *4*, 1148–1153.
(44) Fidelsky, V.; Butera, V.; Zaffran, J.; Toroker, M. C. Three Fundamental Questions on One of Our Best Water Oxidation Catalysts: A Critical Perspective. *Theor. Chem. Acc.* **2016**, *135*, 162.
(45) Doyle, A. D.; Bajdich, M.; Vojvodic, A. Theoretical Insights to Bulk Activity Towards Oxygen Evolution in Oxyhydroxides. *Catal. Letters* **2017**, *147*, 1533–1539.
(46) Tkalych, A. J.; Zhuang, H. L.; Carter, E. A. A Density Functional + U Assessment of Oxygen Evolution Reaction Mechanisms on β-NiOOH. *ACS Catal.* **2017**, *7*, 5329–5339.
(47) Tkalych, A. J.; Zhuang, H. L.; Carter, E. A. Correction to "A Density Functional + U Assessment of Oxygen Evolution Reaction Mechanisms on β-NiOOH." *ACS Catal.* **2018**, *8*, 6070–6070.
(48) Tkalych, A. J.; Martirez, J. M. P.; Carter, E. A. Effect of Transition-Metal-Ion Dopants on the Oxygen Evolution Reaction on NiOOH(0001). *Phys. Chem. Chem. Phys.* **2018**, *20*, 19525–19531.
(49) Govind Rajan, A.; Martirez, J. M. P.; Carter, E. A. Facet-Independent Oxygen Evolution Activity of Pure β-NiOOH: Different Chemistries Leading to Similar Overpotentials. *J. Am. Chem. Soc.* **2020**, *142*, 3600–3612.
(50) Zhou, Y.; López, N. The Role of Fe Species on NiOOH in Oxygen Evolution Reactions. *ACS Catal.* **2020**, *10*, 6254–6261.
(51) Huynh, M. H. V.; Meyer, T. J. Proton-Coupled Electron Transfer. *Chem. Rev.* **2007**, *107*, 5004–5064.
(52) Hammes-Schiffer, S. Theory of Proton-Coupled Electron Transfer in Energy Conversion Processes. *Acc. Chem. Res.* **2009**, *42*, 1881–1889.

(53) Koper, M. T. M. Theory of Multiple Proton–Electron Transfer Reactions and Its Implications for Electrocatalysis. *Chem. Sci.* **2013**, *4*, 2710.
(54) Govind Rajan, A.; Carter, E. A. Discovering Competing Electrocatalytic Mechanisms and their Overpotentials: Automated Enumeration of Oxygen Evolution Pathways. *Submitted*.
(55) Tromans, D. Modeling Oxygen Solubility in Water and Electrolyte Solutions. *Ind. Eng. Chem. Res.* **2000**, *39*, 805–812.
(56) Bandura, A. V.; Lvov, S. N. The Ionization Constant of Water over Wide Ranges of Temperature and Density. *J. Phys. Chem. Ref. Data* **2006**, *35*, 15–30.
(57) Davis, R. E.; Horvath, G. L.; Tobias, C. W. The Solubility and Diffusion Coefficient of Oxygen in Potassium Hydroxide Solutions. *Electrochim. Acta* **1967**, *12*, 287–297.
(58) Martirez, J. M. P.; Carter, E. A. Effects of the Aqueous Environment on the Stability and Chemistry of β-NiOOH Surfaces. *Chem. Mater.* **2018**, *30*, 5205–5219.
(59) Franck–Condon Principle. In *IUPAC Compendium of Chemical Terminology, 2nd ed. (the "Gold Book")*; McNaught, A. D.; Wilkinson, A., Eds.; Blackwell Scientific Publications: Oxford, 1997.
(60) Cukierman, S. Et Tu, Grotthuss! And Other Unfinished Stories. *Biochim. Biophys. Acta - Bioenerg.* **2006**, *1757*, 876–885.
(61) Trześniewski, B. J.; Diaz-Morales, O.; Vermaas, D. A.; Longo, A.; Bras, W.; Koper, M. T. M.; Smith, W. A. In Situ Observation of Active Oxygen Species in Fe-Containing Ni-Based Oxygen Evolution Catalysts: The Effect of pH on Electrochemical Activity. *J. Am. Chem. Soc.* **2015**, *137*, 15112–15121.
(62) Garcia, A. C.; Touzalin, T.; Nieuwland, C.; Perini, N.; Koper, M. T. M. Enhancement of Oxygen Evolution Activity of Nickel Oxyhydroxide by Electrolyte Alkali Cations. *Angew. Chemie* **2019**, *131*, 13133–13137.
(63) Li, L.-F.; Li, Y.-F.; Liu, Z.-P. Oxygen Evolution Activity on NiOOH Catalysts: Four-Coordinated Ni Cation as the Active Site and the Hydroperoxide Mechanism. *ACS Catal.* **2020**, *10*, 2581–2590.
(64) Chen, L.; Dong, X.; Wang, Y.; Xia, Y. Separating Hydrogen and Oxygen Evolution in Alkaline Water Electrolysis Using Nickel Hydroxide. *Nat. Commun.* **2016**, *7*, 11741.
(65) Rohatgi, A. WebPlotDigitizer Version 3.9, 2015, https://apps.automeris.io/wpd/ (last accessed: June 2020).